Journal of Computational Physics 300 (2015) 202–218

Contents lists available at ScienceDirect

Journal of Computational Physics

www.elsevier.com/locate/jcp

Well-balanced central-upwind scheme for a fully coupled shallow water system modeling flows over erodible bed

Xin Liu [a,*], Abdolmajid Mohammadian [a], Alexander Kurganov [b], Julio Angel Infante Sedano [a]

[a] Department of Civil Engineering, University of Ottawa, Ottawa, ON K1N6N5, Canada
[b] Mathematics Department, Tulane University, New Orleans, LA 70118, USA

ARTICLE INFO

Article history:
Received 30 September 2014
Received in revised form 15 July 2015
Accepted 23 July 2015
Available online 31 July 2015

Keywords:
Fully coupled shallow water system
Sediment transport
Dam-break flow
Finite-volume method
Well-balanced central-upwind scheme
Lagrange theorem

ABSTRACT

Intense sediment transport and rapid bed evolution are frequently observed under highly-energetic flows, and bed erosion sometimes is of the same magnitude as the flow itself. Simultaneous simulation of multiple physical processes requires a fully coupled system to achieve an accurate hydraulic and morphodynamical prediction. In this paper, we develop a high-order well-balanced finite-volume method for a new fully coupled two-dimensional hyperbolic system consisting of the shallow water equations with friction terms coupled with the equations modeling the sediment transport and bed evolution.

The nonequilibrium sediment transport equation is used to predict the sediment concentration variation. Since bed-load, sediment entrainment and deposition have significant effects on the bed evolution, an Exner-based equation is adopted together with the Grass bed-load formula and sediment entrainment and deposition models to calculate the morphological process. The resulting 5×5 hyperbolic system of balance laws is numerically solved using a Godunov-type central-upwind scheme on a triangular grid. A computationally expensive process of finding all of the eigenvalues of the Jacobian matrices is avoided: The upper/lower bounds on the largest/smallest local speeds of propagation are estimated using the Lagrange theorem. A special discretization of the bed-slope term is proposed to guarantee the well-balanced property of the designed scheme. The proposed fully coupled model is verified on a number of numerical experiments.

1. Introduction

Shallow water systems are widely used in predicting hydrodynamics of surface flows such as water flows in rivers, channels, flood plains and coastal regions. It is well-known that the shallow water systems can accurately predict the hydraulic parameters under conditions of slow erosion and low sediment concentration. However, in cases of highly energetic flows like dam-break or flood flows, the effects of intense sediment exchange and rapid bed evolution cannot be neglected.

In recent years, a number of dam-break hydraulics models have been developed to predict the fluid flow and sediment transport [37,44,46,47,59,60]. However, the majority of the current models are based on the decoupled equations of flow and sediment transport and thus they are restricted to erosion rates which are considerably weaker than the flow, see, e.g.,

* Corresponding author.
E-mail addresses: liuxin429go@gmail.com (X. Liu), majid.mohammadian@uottawa.ca (A. Mohammadian), kurganov@math.tulane.edu (A. Kurganov), jinfante@uottawa.ca (J.A. Infante Sedano).

http://dx.doi.org/10.1016/j.jcp.2015.07.043
0021-9991/

[37,56]. However, dam-break flows may induce intense sediment transport and rapid morphological changes which are not independent processes but have mutually significant interactions with the fluid flow. In many dam-break cases and in strong fluvial processes in rivers, the bed evolution is almost of the same order of magnitude as the free-surface level changes [55]. Hence, developing a dam-break model that takes into account coupling hydraulic model with the sediment transport and bed evolution equations is required in such cases.

Many dam-break models based on fixed-bed conditions have been developed, see, e.g., [6–8,44,47,59,60]. In order to evaluate morphological changes during the high-energy dam-break flows, some earlier numerical models use uncoupled strategy to first solve the hydrodynamic model, and then to solve the sediment transport and bed deformation equations separately, see, e.g., [19,20,41,46]. More recently, noting that the flow, sediment transport and bed evolution can be strongly coupled to each other while the rate of bed deformation being considerable compared to that of the flow evolution, several coupled mathematical modeling strategies for simulating dam-break flows over mobile beds have been developed. Fagherazzi and Sun [17] presented a 1-D coupled system consisting of a simplified shallow water system, sediment concentration and bed level calculation. Cao et al. [11] proposed a 1-D coupled model and the sediment entrainment and deposition are considered to update the bed-levels. Wu and Wang presented a similar 1-D coupled model for dam-break flows over erodible beds in [51] including the bed-load transport. Capart and Young [12] developed a one-dimensional (1-D) coupled dam-break model based on an explicit finite-difference algorithm.

Several two-dimensional (2-D) coupled models for dam-break flows over mobile beds have been recently introduced. Simpson and Castelltort [43] presented a 2-D model for the free surface flow, sediment transport and bed level change based on the 1-D model from [11]. Yue et al. [54] extended the 1-D model from [11] to 2-D for modeling alluvial processes with intense sediment transport and rapid bed evolution. Similar 2-D coupled mathematical models have been also studied in [24,52]. Li and Duffy [36] proposed a fully coupled 2-D system including the modified shallow water system, sediment transport and bed evolution. In their study, the bed evolution formula is rewritten to couple the sediment entrainment and deposition effects by substituting the sediment transport equation into it. Meanwhile, the sediment exchange terms are treated as source terms which will not affect the solution of the hyperbolic system. In [5], Benkhaldoun et al. presented a coupled 2-D model, which consists of both bed-load and sediment exchange in the morphological equation, and the bed-load terms are treated as a flux term coupled in the hyperbolic system. Hudson and Sweby [25] investigated the accuracy and determined the validity of both the steady approach and unsteady approach of five different types of governing formulations coupling the morphology continuity equation on rectangular meshes. They concluded that one conservative reformulation form based on the unsteady approach was overall the best. However, the drawback of this form is its dependence of the Jacobian matrix on z, which was shown and discussed in [42]. Castro Díaz et al. [13] studied the numerical approximation of bed-load sediment transport due to shallow layer flows on unstructured meshes with a second-order MUSCL-type reconstruction. Murillo and Garcia-Navarro [39] studied an Exner-based coupled model for 2-D transient flows over erodible beds on triangular unstructured meshes and developed a general “Grass formula” format expressing several commonly used empirical bed-load formulas. A similar scheme is adopted in the current study using the Meyer–Peter and Müller formula. Soares-Frazão and Zech [45] built a coupled system using the HLLC method and proposed an approximate analytical expression for the wave celerities, which was valid for any Froude number.

In this paper, we propose a new fully coupled hyperbolic system consisting of hydrodynamic model, sediment transport and morphological evolution. The obtained hyperbolic system of balance laws consists of five coupled equations, for which no analytical expressions for the eigenstructure are available. This makes it difficult to develop a robust and efficient upwind scheme for the proposed model. We develop a Riemann-problem-solver-free finite volume method for the studied fully coupled system. Our method is based on the efficient, robust and highly accurate semi-discrete central-upwind scheme, originally introduced in [28–30,33] for general multidimensional hyperbolic systems of conservation laws. The central-upwind scheme was first extended to the Saint-Venant system of shallow water equations in [27]. A more robust, well-balanced and positivity preserving central-upwind scheme for the shallow water equations was developed on both Cartesian [31] and triangular [8] grids. These schemes are capable of exactly preserving “lake at rest” steady-state solutions and preserving positivity of the computed water depth. In this paper, we extend the second-order semi-discrete central-upwind scheme to the fully coupled shallow water system modeling flows over erodible bed. Since, according to the central-upwind methodology, no (generalized) Riemann problems are to be (approximately) solved, the numerical fluxes are obtained in a straightforward manner. The one-sided local speeds needed to evaluate numerical fluxes are estimated using the Lagrange theorem [34,38], which significantly reduces the numerical cost (the same approach was used in [14,32] in the context of the two- and three-layer shallow water equations). We complete the development of the well-balanced (in the sense that it is capable of exactly preserving “lake at rest” states) central-upwind scheme by designing a positivity preserving piecewise linear reconstruction and a well-balanced quadrature for the bed-slope terms.

This paper is organized as follows. In Section 2, we present the governing equations, for which in Section 3 we develop the central-upwind scheme. Several numerical experiments are then presented in Section 4. Some concluding remarks complete the paper in Section 5.

2. Governing equations

In this section, we will present the model equations (Section 2.1) and write down the studied model in the vector form (Section 2.2).

2.1. Fully coupled shallow water system modeling flows over erodible bed

We follow the approach in [11] and modify the continuity equation to account for the sediment effect. As in the 1-D model from [51], we consider both bed-load and suspended load effects in the momentum equations. The resulting 2-D modified shallow water equations read:

$$h_t + (hu)_x + (hv)_y = -Z_t, \tag{1}$$

$$(hu)_t + \left(hu^2 + \frac{g}{2}h^2\right)_x + (huv)_y = -gh(Z_x + S_f^x), \tag{2}$$

$$(hv)_t + (huv)_x + \left(hv^2 + \frac{g}{2}h^2\right)_y = -gh(Z_y + S_f^y). \tag{3}$$

The sediment transportation and morphological evolution are modeled based on the mass and momentum conversation of sediment and water–sediment mixture. We model the bed evolution using an Exner-based equation proposed in [23], which we modify to comprise both bed-load and suspended-load. The 2-D sediment transport equation for total load and the morphological evolution equation is given by

$$(hc)_t + (huc)_x + (hvc)_y = E - D \tag{4}$$

and

$$Z_t + \frac{\mu}{1-p}\left[u\left(u^2+v^2\right)\right]_x + \frac{\mu}{1-p}\left[v\left(u^2+v^2\right)\right]_y = -\frac{E-D}{1-p}, \tag{5}$$

respectively.

In equations (1)–(5), t is time, x and y are horizontal coordinates. The unknown functions are the water depth $h = h(x, y, t)$, the x- and y-components of the depth-averaged velocity, $u = u(x, y, t)$ and $v = v(x, y, t)$, respectively, the volumetric sediment concentration $c = c(x, y, t)$, and the bed elevation $Z = Z(x, y, t)$. The following quantities are parameters of the model: g is the gravitational acceleration; p is the bed porosity; μ is a coefficient usually obtained experimentally by taking into account the grain diameter and the kinematic viscosity of the sediment mixture; E and D are sediment entrainment and deposition fluxes across the bottom boundary of flow, which represent the sediment exchange between the bed and water column; S_f^x and S_f^y are friction slope terms in the x- and y-directions, respectively, which are computed using Manning's roughness coefficient n_b as follows: $S_f^x = n_b^2 u\sqrt{u^2+v^2}/h^{4/3}$, $S_f^y = n_b^2 v\sqrt{u^2+v^2}/h^{4/3}$. In all of our numerical experiments, we set $n_b = 0.02$.

Bed sediment entrainment due to turbulence, E, and sediment deposition due to gravity, D, are two distinct mechanisms involved in the sediment exchange and bed evolution processes. And they are considered for source of suspended sediment in the current study. Several empirical formulations derived on various premises were reviewed in [10,11]. We adopted the formulas used in [11], where the coefficients in E and D were determined based on non-cohesive sediment assumptions. First,

$$D := \omega_0 (1 - C_a)^m C_a, \tag{6}$$

where ω_0 is the settling velocity of a single particle in tranquil water, which can be calculated as:

$$\omega_0 = \sqrt{(13.95\nu/d)^2 + 1.09sgd} - 13.95\nu/d. \tag{7}$$

In formulas (6), (7), ν is the kinematic viscosity of water ($\nu = 1.2 \times 10^{-6}$), d is the average diameter of sediment particles, s is the submerged specific gravity of sediment given by $s = \frac{\rho_s}{\rho_f} - 1$, where ρ_s is the density of sediment particles and ρ_f is the density of clear water; m is an exponent indicating the effects of hindered settling due to high sediment concentration, C_a is the local near-bed sediment concentration in volume, which can be determined by $C_a = \alpha c$, where the coefficient α is usually larger than 1 and must not exceed $(1-p)$. α is empirically specified by $\alpha = \min[2, (1-p)/c]$. And E is calculated as:

$$E := \begin{cases} \dfrac{\varphi(\theta - \theta_c)\sqrt{u^2+v^2}}{h d^{1/5}}, & \text{if } \theta \geq \theta_c, \\ 0, & \text{otherwise.} \end{cases}$$

Here, φ is a coefficient to control the erosion force (in our numerical examples, we take $\varphi = 0.015$), θ is the dimensionless shear stress which can be calculated as $\theta = hS_f/(sd)$, and θ_c is the critical Shields parameter for initiation of sediment movement (the commonly used value is experimentally determined as $\theta_c = 0.047$).

2.2. Vector form of the fully coupled shallow water system

In order to make it easier to design a well-balanced scheme for the studied fully coupled shallow water system, we introduce the water surface variable $\eta := h + Z$ and rewrite the system (1)–(5) in terms of the equilibrium variables $\boldsymbol{U} := (\eta, hu, hv, hc, Z)^T$ in the following vector form:

$$\boldsymbol{U}_t + \boldsymbol{F}_x + \boldsymbol{G}_y = \boldsymbol{S} + \boldsymbol{K}. \tag{8}$$

Here, $\boldsymbol{F}$ and $\boldsymbol{G}$ are:

$$\boldsymbol{F}=\begin{pmatrix} hu \\ \frac{(hu)^2}{\eta-Z}+\frac{g}{2}\eta^2-g\eta Z \\ \frac{(hu)(hv)}{\eta-Z} \\ \frac{(hu)(hc)}{\eta-Z} \\ \frac{\mu}{1-p}\frac{(hu)\left[(hu)^2+(hv)^2\right]}{(\eta-Z)^3} \end{pmatrix},\quad \boldsymbol{G}=\begin{pmatrix} hv \\ \frac{(hu)(hv)}{\eta-Z} \\ \frac{(hv)^2}{\eta-Z}+\frac{g}{2}\eta^2-g\eta Z \\ \frac{(hv)(hc)}{\eta-Z} \\ \frac{\mu}{1-p}\frac{(hv)\left[(hu)^2+(hv)^2\right]}{(\eta-Z)^3} \end{pmatrix}, \tag{9}$$

and $\boldsymbol{S}$ and $\boldsymbol{K}$ are:

$$\boldsymbol{S}=\begin{pmatrix} 0 \\ -g\eta Z_x \\ -g\eta Z_y \\ 0 \\ 0 \end{pmatrix},\quad \boldsymbol{K}=\begin{pmatrix} 0 \\ -g(\eta-Z)S_f^x \\ -g(\eta-Z)S_f^y \\ E-D \\ -\frac{E-D}{1-p} \end{pmatrix}. \tag{10}$$

In order to define a quasi-linear hyperbolic system, the geometric source term $\boldsymbol{S}=P(\boldsymbol{U})\boldsymbol{U}_x+Q(\boldsymbol{U})\boldsymbol{U}_y$ is incorporated into the Jacobian matrix following the approach in [39,42]. Notice that, for smooth solutions, the system (8)–(10) can be rewritten in the following form:

$$\boldsymbol{U}+\left[A(\boldsymbol{U})-P(\boldsymbol{U})\right]\boldsymbol{U}_x+\left[B(\boldsymbol{U})-Q(\boldsymbol{U})\right]\boldsymbol{U}_y=\boldsymbol{K},$$

where

$$A(\boldsymbol{U})=\begin{pmatrix} 0 & 1 & 0 & 0 & 0 \\ -\frac{(hu)^2}{(\eta-Z)^2}+g(\eta-Z) & \frac{2hu}{\eta-Z} & 0 & 0 & \frac{(hu)^2}{(\eta-Z)^2} \\ -\frac{(hu)(hv)}{(\eta-Z)^2} & \frac{hv}{\eta-Z} & \frac{hu}{\eta-Z} & 0 & \frac{(hu)(hv)}{(\eta-Z)^2} \\ -\frac{(hu)(hc)}{(\eta-Z)^2} & \frac{hc}{\eta-Z} & 0 & \frac{hu}{\eta-Z} & \frac{(hu)(hc)}{(\eta-Z)^2} \\ -3\frac{\mu}{1-p}\frac{(hu)[(hu)^2+(hv)^2]}{(\eta-Z)^4} & \frac{\mu}{1-p}\frac{3(hu)^2+(hv)^2}{(\eta-Z)^3} & \frac{\mu}{1-p}\frac{2(hu)(hu)}{(\eta-Z)^3} & 0 & 3\frac{\mu}{1-p}\frac{(hu)[(hu)^2+(hv)^2]}{(\eta-Z)^4} \end{pmatrix}, \tag{11}$$

$$B(\boldsymbol{U})=\begin{pmatrix} 0 & 0 & 1 & 0 & 0 \\ -\frac{(hu)(hv)}{(\eta-Z)^2} & \frac{hv}{\eta-Z} & \frac{hu}{\eta-Z} & 0 & \frac{(hu)(hv)}{(\eta-Z)^2} \\ -\frac{(hv)^2}{(\eta-Z)^2}+g(\eta-Z) & 0 & \frac{2hv}{\eta-Z} & 0 & \frac{(hv)^2}{(\eta-Z)^2} \\ -\frac{(hv)(hc)}{(\eta-Z)^2} & 0 & \frac{hc}{\eta-Z} & \frac{hv}{\eta-Z} & \frac{(hv)(hc)}{(\eta-Z)^2} \\ -3\frac{\mu}{1-p}\frac{(hv)[(hu)^2+(hv)^2]}{(\eta-Z)^4} & \frac{\mu}{1-p}\frac{2(hu)(hv)}{(\eta-Z)^3} & \frac{\mu}{1-p}\frac{3(hv)^2+(hu)^2}{(\eta-Z)^3} & 0 & 3\frac{\mu}{1-p}\frac{(hv)[(hu)^2+(hv)^2]}{(\eta-Z)^4} \end{pmatrix}, \tag{12}$$

and

$$P(\boldsymbol{U})=\begin{pmatrix} 0&0&0&0&0 \\ 0&0&0&0&-g\eta \\ 0&0&0&0&0 \\ 0&0&0&0&0 \\ 0&0&0&0&0 \end{pmatrix},\quad Q(\boldsymbol{U})=\begin{pmatrix} 0&0&0&0&0 \\ 0&0&0&0&0 \\ 0&0&0&0&-g\eta \\ 0&0&0&0&0 \\ 0&0&0&0&0 \end{pmatrix}. \tag{13}$$

3. Semi-discrete central-upwind scheme

We now turn to the derivation of the semi-discrete central-upwind scheme for the system (8)–(10).

We assume that an unstructured triangulation $\mathcal{T}:=\bigcup_i T_i$ of the computational domain, consisting of triangular cells T_i of size $|T_i|$, is given. We denote by $\boldsymbol{n}_{ik}:=(\cos(\theta_{ik}),\sin(\theta ik))^T$ the outer unit normals to the corresponding sides of T_i of length ℓ_{ik}, $k=1,2,3$, see Fig. 1. Let (x_i,y_i) be the coordinates of the centroid of T_i and $M_{ik}=(x_{ik},y_{ik})$ be the midpoint of

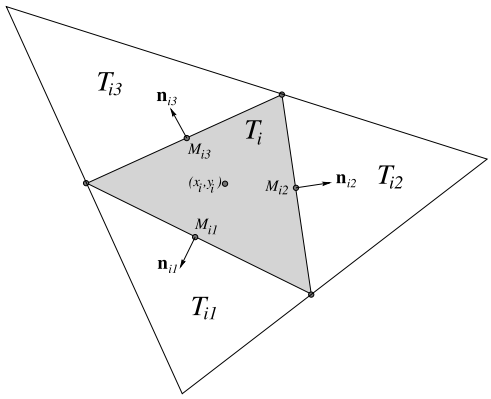

Fig. 1. A typical triangular cell with three neighbors.

the k-th side of the triangle T_i, $k = 1, 2, 3$. We denote by T_{i1}, T_{i2} and T_{i3} the neighboring triangles that share a common side with T_i.

A semi-discrete scheme for (8)–(10) is a system of ODEs for the approximations of the cell averages of the solution:

$$\overline{\boldsymbol{U}}_i(t) \approx \frac{1}{|T_i|}\int\limits_{T_i} \boldsymbol{U}(x, y, t)\,dxdy.$$

We refer the reader to [30], where a general form of a "triangular" central-upwind scheme for systems of hyperbolic conservation laws is derived. We follow [8,30] and obtain the semi-discrete second-order central-upwind scheme, which reads:

$$\begin{aligned}\frac{d\,\overline{\boldsymbol{U}}_i}{dt} = &-\frac{1}{|T_i|}\sum_{k=1}^{3}\frac{\ell_{ik}\cos(\theta_{ik})}{a^{\text{in}}_{ik}+a^{\text{out}}_{ik}}\Big[a^{\text{in}}_{ik}\boldsymbol{F}(\boldsymbol{U}_{ik}(M_{ik})) + a^{\text{out}}_{ik}\boldsymbol{F}(\boldsymbol{U}_i(M_{ik}))\Big]\\ &-\frac{1}{|T_i|}\sum_{k=1}^{3}\frac{\ell_{ik}\sin(\theta_{ik})}{a^{\text{in}}_{ik}+a^{\text{out}}_{ik}}\Big[a^{\text{in}}_{ik}\boldsymbol{G}(\boldsymbol{U}_{ik}(M_{ik})) + a^{\text{out}}_{ik}\boldsymbol{G}(\boldsymbol{U}_i(M_{ik}))\Big]\\ &+\frac{1}{|T_i|}\sum_{k=1}^{3}\ell_{ik}\frac{a^{\text{in}}_{ik}a^{\text{out}}_{ik}}{a^{\text{in}}_{ik}+a^{\text{out}}_{ik}}\Big[\boldsymbol{U}_{ik}(M_{ik}) - \boldsymbol{U}_i(M_{jk})\Big] + \overline{\boldsymbol{S}}_i + \overline{\boldsymbol{K}}_i.\end{aligned} \tag{14}$$

Here, $\boldsymbol{U}_i(M_{ik})$ and $\boldsymbol{U}_{ik}(M_{ik})$ are the corresponding values at M_{ik} of the piecewise linear reconstruction

$$\mathring{\boldsymbol{U}}(x, y) := \overline{\boldsymbol{U}}_i + (\widehat{\boldsymbol{U}}_x)_i(x - x_i) + (\widehat{\boldsymbol{U}}_y)_i(y - y_i), \quad (x, y) \in T_i \tag{15}$$

of $\boldsymbol{U}$ at time t, that is:

$$\boldsymbol{U}_i(M_{ik}) := \lim_{(x,y)\to M_{ik};(x,y)\in T_i}\mathring{\boldsymbol{U}}(x, y), \qquad \boldsymbol{U}_{ik}(M_{ik}) := \lim_{(x,y)\to M_{ik};(x,y)\in T_{ik}}\mathring{\boldsymbol{U}}(x, y), \tag{16}$$

where the numerical derivatives $(\widehat{\boldsymbol{U}}_x)_i$ and $(\widehat{\boldsymbol{U}}_y)_i$ are (at least) first-order, componentwise approximations of $\boldsymbol{U}_x(x_i, y_i, t)$ and $\boldsymbol{U}_y(x_i, y_i, t)$, respectively, computed via a nonlinear limiter used to minimize the oscillations of the reconstruction (15), see Section 3.1.

The directional local speeds a^{in}_{ik} and a^{out}_{ik} in (14) are defined by

$$\begin{aligned}a^{\text{in}}_{ik}(M_{ik}) &= -\min\{\lambda_1[V_{ik}(\boldsymbol{U}_i(M_{ik}))],\ \lambda_1[V_{ik}(\boldsymbol{U}_{ik}(M_{ik})],\ 0\},\\ a^{\text{out}}_{ik}(M_{ik}) &= \max\{\lambda_5[V_{ik}(\boldsymbol{U}_i(M_{ik}))],\ \lambda_5[V_{ik}(\boldsymbol{U}_{ik}(M_{ik})],\ 0\},\end{aligned} \tag{17}$$

where $\lambda_1[V_{ik}] \le \ldots \le \lambda_5[V_{ik}]$ are the eigenvalues of the matrices

$$\begin{aligned}V_{ik}(\boldsymbol{U}_i(M_{ik})) := &\cos(\theta_{ik})\Big[A(\boldsymbol{U}_i(M_{ik})) + P(\boldsymbol{U}_i(M_{ik}))\Big]\\ &+ \sin(\theta_{ik})\Big[B(\boldsymbol{U}_i(M_{ik})) + Q(\boldsymbol{U}_i(M_{ik}))\Big],\end{aligned} \tag{18}$$

and

$$\begin{aligned}V_{ik}(\boldsymbol{U}_{ik}(M_{ik})) := &\cos(\theta_{ik})\Big[A(\boldsymbol{U}_{ik}(M_{ik})) + P(\boldsymbol{U}_{ik}(M_{ik}))\Big]\\ &+ \sin(\theta_{ik})\Big[B(\boldsymbol{U}_{ik}(M_{ik})) + Q(\boldsymbol{U}_{ik}(M_{ik}))\Big],\end{aligned} \tag{19}$$

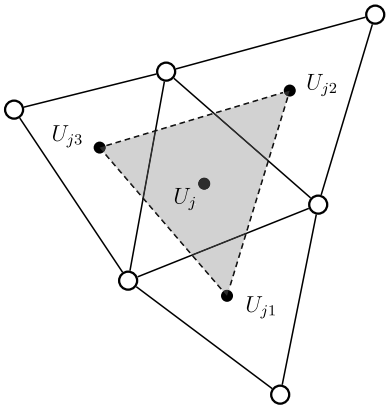

Fig. 2. Stencil for calculating nonlimited derivatives.

where A, B, P and Q are given by (11)–(13). Unfortunately, no analytical expressions for $\lambda_1[V_{ik}]$ and $\lambda_5[V_{ik}]$ are available. We therefore follow the approach in [14,32] and establish a lower bound for $\lambda_1[V_{ik}]$ and an upper bound for $\lambda_5[V_{ik}]$ using the Lagrange theorem [34,38], see Section 3.2.

Finally, $\overline{\boldsymbol{S}}_i$ and $\overline{\boldsymbol{K}}_i$ in (14) are the cell averages of the bed-slope term $\boldsymbol{S}$ and the source term $\boldsymbol{K}$, respectively, over the cell T_i.

3.1. Non-oscillatory piecewise linear reconstruction

In this section, we describe a nonlinear limiter used to evaluate the numerical derivatives $(\widehat{\boldsymbol{U}}_x)_i$ and $(\widehat{\boldsymbol{U}}_y)_i$ in (15) in a non-oscillatory manner. A variety of limiters on triangular grids can be found in, for example, [1,8,15,16,26,30,40,50]. In the present study, the limiting approach proposed by Jawahar and Kamath in [26] is adopted.

First, we compute the nonlimited gradients $(\nabla \boldsymbol{U})_j$ in every cell T_j by taking the x- and y-derivatives of the planes passing through the points $(x_{j1}, y_{j1}, \boldsymbol{U}_{j1})$, $(x_{j2}, y_{j2}, \boldsymbol{U}_{j2})$ and $(x_{j3}, y_{j3}, \boldsymbol{U}_{j3})$ outlined in Fig. 2:

$$
\begin{aligned}
(\boldsymbol{U}_x)_j &= \frac{(y_{j3}-y_{j1})(\boldsymbol{U}_{j2}-\boldsymbol{U}_{j1})-(y_{j2}-y_{j1})(\boldsymbol{U}_{j3}-\boldsymbol{U}_{j1})}{(y_{j3}-y_{j1})(x_{j2}-x_{j1})-(y_{j2}-y_{j1})(x_{j3}-x_{j1})},\\
(\boldsymbol{U}_y)_j &= \frac{(x_{j2}-x_{j1})(\boldsymbol{U}_{j3}-\boldsymbol{U}_{j1})-(x_{j3}-y_{j1})(\boldsymbol{U}_{j2}-\boldsymbol{U}_{j1})}{(x_{j2}-x_{j1})(y_{j3}-y_{j1})-(x_{j3}-x_{j1})(y_{j2}-y_{j1})}.
\end{aligned}
\tag{20}
$$

We then follow the approach in [40] and obtain the limited numerical gradient $(\nabla\widehat{\boldsymbol{U}})_i$ by taking the weighted average of three nonlimited gradients:

$$
(\nabla\widehat{\boldsymbol{U}})_i = \Lambda_{i1}(\nabla\boldsymbol{U})_{i1} + \Lambda_{i2}(\nabla\boldsymbol{U})_{i2} + \Lambda_{i3}(\nabla\boldsymbol{U})_{i3}, \tag{21}
$$

where Λ_{i1}, Λ_{i2} and Λ_{i3} are weights and $(\nabla\boldsymbol{U})_{i1}$, $(\nabla\boldsymbol{U})_{i2}$ and $(\nabla\boldsymbol{U})_{i3}$ are the three nonlimited gradients computed using (20) for $j = i1$, $i2$ and $i3$, respectively.

The weights are calculated as follows:

$$
\begin{aligned}
\Lambda_{i1} &= \frac{\|(\nabla\boldsymbol{U})_{i2}\|_2^2\|(\nabla\boldsymbol{U})_{i3}\|_2^2+\varepsilon}{\|(\nabla\boldsymbol{U})_{i1}\|_2^4+\|(\nabla\boldsymbol{U})_{i2}\|_2^4+\|(\nabla\boldsymbol{U})_{i3}\|_2^4+3\varepsilon},\\
\Lambda_{i2} &= \frac{\|(\nabla\boldsymbol{U})_{i1}\|_2^2\|(\nabla\boldsymbol{U})_{i3}\|_2^2+\varepsilon}{\|(\nabla\boldsymbol{U})_{i1}\|_2^4+\|(\nabla\boldsymbol{U})_{i2}\|_2^4+\|(\nabla\boldsymbol{U})_{i3}\|_2^4+3\varepsilon},\\
\Lambda_{i3} &= \frac{\|(\nabla\boldsymbol{U})_{i1}\|_2^2\|(\nabla\boldsymbol{U})_{i2}\|_2^2+\varepsilon}{\|(\nabla\boldsymbol{U})_{i1}\|_2^4+\|(\nabla\boldsymbol{U})_{i2}\|_2^4+\|(\nabla\boldsymbol{U})_{i3}\|_2^4+3\varepsilon},
\end{aligned}
$$

where the parameter ε is a small positive number introduced to prevent division by zero. In all of the numerical examples presented in Section 4, we have taken $\varepsilon = 10^{-14}$.

Equipped with the numerical gradient (21), we obtain the piecewise linear approximations (15) for each of the conservative variables. These approximants $\mathring{\boldsymbol{U}}(x, y)$ are to be used to evaluate the point values of $\boldsymbol{U}$ at the midpoints of the cell edges, M_{ik}. To prevent appearance of any negative water depth values at these points, we replace the corresponding point values of the bottom elevation with

$$
\mathring{U}^{(5)}(M_{ik}) := \min(\mathring{U}^{(5)}(M_{ik}), \mathring{U}^{(1)}(M_{ik})).
$$

3.2. Estimating one-sided local speeds of propagation

We now turn to establishing an upper bound on the largest eigenvalue and a lower bound on the smallest eigenvalue of the matrices $V_{ik}(\boldsymbol{U}_i(M_{ik}))$ and $V_{ik}(\boldsymbol{U}_{ik}(M_{ik}))$ given by (18) and (19), respectively.

To this end, we employ the following theorem originally introduced by Lagrange in [34], see also [38] for the proof of the theorem and precise description on the way to obtain an upper bound on the largest positive root of a polynomial. The Lagrange theorem can be formulated as follows:

Let $P_n(\lambda) = \lambda^n + b_1\lambda^{n-1} + \ldots + b_{n-1}\lambda + b_n$ be a nonconstant polynomial of degree n. Then, the largest nonnegative root of P_n is smaller than the sum of the largest and the second largest numbers in the set $\{|b_j|^{1/j} : b_j \in J_{\max}\}$, where $J_{\max}$ is the set of the negative coefficients of P_n.

For the matrices $V_{ik}(\boldsymbol{U}_i(M_{ik}))$ and $V_{ik}(\boldsymbol{U}_{ik}(M_{ik}))$, the characteristic polynomials read

$$\left[\lambda^4 + b_1\lambda^3 + b_2\lambda^2 + b_3\lambda + b_4\right]\left(\frac{hu}{\eta - Z}\cos(\theta_{ik}) + \frac{hv}{\eta - Z}\sin(\theta_{ik}) - \lambda\right), \tag{22}$$

where the coefficients b_1, b_2, b_3 and b_4 can be written explicitly using the definitions of the matrices A and B given by (11) and (12), respectively (we do not provide the expressions of these coefficients for the sake of brevity).

Then, $a_{ik}^{\text{out}}(M_{ik})$ is obtained using the upper bound of the largest nonnegative root of the fourth-order polynomial in the square brackets in equation (22), which is obtained using the Lagrange theorem. Similarly, $a_{ik}^{\text{in}}(M_{ik})$ is obtained using a lower bound on the smallest nonpositive root of the fourth-order polynomial in the square bracket in equation (22) (according to the Lagrange theorem, this root is larger than the sum of the smallest and second smallest numbers in the set $\{-|d_j|^{1/j} : b_j \in J_{\min}\}$, where $J_{\min}$ is the set of the negative coefficients of the polynomial $\lambda^4 + d_1\lambda^3 + d_2\lambda^2 + d_3\lambda + b_4$ with $d_j = (-1)^j b_j$, $\forall j$).

3.3. Well-balanced discretization of the bed-slope terms

In this section, we describe a well-balanced discretization of the bed-slope terms, which guarantees that "lake at rest" solutions that satisfy

$$\eta \equiv \eta_c = \text{Const}, \quad u \equiv v \equiv 0, \tag{23}$$

are exactly preserved by the resulting central-upwind scheme. Notice that unlike the case of the classical Saint-Venant system, the "lake at rest" state in the current study is not a steady-state solution since both hc and Z variables may change in time while the identities (23) are satisfied. However, the "lake at rest" state is still physically significant and the approach of designing a special well-balanced quadrature for the geometric source term proposed in [8] can be extended to the studied system (8)–(10) so that the identities (23) are satisfied by the computed solution provided they are satisfied by the initial data.

First, we note that the second and third components of the source term K vanish at "lake at rest" states and therefore, the well-balanced property of the scheme will be guaranteed if the discretized cell average of the geometric term $\overline{\boldsymbol{S}}_i$, exactly balances the rest of numerical fluxes so that the second and third components on the right-hand side (RHS) of (14) vanish for the data satisfying (23).

After a substitution of a "lake at rest" state into (14), we conclude that a well-balanced quadrature of S should satisfy the following two conditions:

$$-\frac{g}{|T_i|}\sum_{k=1}^{3}\ell_{ik}\cos(\theta_{ik})\left[\frac{\eta_c^2}{2} - \eta_c\frac{a_{ik}^{\text{in}}Z_{ik}(M_{ik}) + a_{ik}^{\text{out}}Z_i(M_{ik})}{a_{ik}^{\text{in}} + a_{ik}^{\text{out}}}\right] + \overline{S}_i^{(2)} = 0 \tag{24}$$

and

$$-\frac{g}{|T_i|}\sum_{k=1}^{3}\ell_{ik}\sin(\theta_{ik})\left[\frac{\eta_c^2}{2} - \eta_c\frac{a_{ik}^{\text{in}}Z_{ik}(M_{ik}) + a_{ik}^{\text{out}}Z_i(M_{ik})}{a_{ik}^{\text{in}} + a_{ik}^{\text{out}}}\right] + \overline{S}_i^{(3)} = 0, \tag{25}$$

where

$$\overline{S}_i^{(2)} \approx -\frac{g}{|T_i|}\int\limits_{T_i}\eta Z_x\,dxdy, \qquad \overline{S}_i^{(3)} \approx -\frac{g}{|T_i|}\int\limits_{T_i}\eta Z_y\,dxdy.$$

To derive the desired well-balanced quadrature, we first apply Green's formula,

$$\int\limits_{T_i}\operatorname{div}\boldsymbol{\mathcal{G}}\,dxdy = \int\limits_{\partial T_i}\boldsymbol{\mathcal{G}}\cdot\boldsymbol{n}\,ds,$$

to the vector field $\mathcal{G} = (\frac{1}{2}\eta^2 - \eta Z, 0)$ and obtain:

$$-\int\limits_{T_i} \eta Z_x \, dxdy = \sum_{k=1}^{3} \int\limits_{(\partial T_i)_k} \left(\frac{\eta^2}{2} - \eta Z\right) \cos(\theta_{ik}) \, ds - \int\limits_{T_i} (\eta - Z)\eta_x \, dxdy, \tag{26}$$

where $(\partial T_i)_k$ is the k-th side of the triangle T_i, $k = 1, 2, 3$. We then apply the midpoint rule to the integrals on the RHS of (26) and obtain

$$\begin{aligned}\overline{S}_i^{(2)} &= -g(\overline{\eta}_i - \overline{Z}_i)\eta_x(x_i, y_i) \\ &\quad + \frac{g}{|T_i|} \sum_{k=1}^{3} \ell_{ik} \cos(\theta_{ik}) \frac{a_{ik}^{\text{in}} \left(\frac{\eta_{ik}^2(M_{ik})}{2} - \eta_{ik}(M_{ik}) Z_{ik}(M_{ik})\right) + a_{ik}^{\text{out}} \left(\frac{\eta_i^2(M_{ik})}{2} - \eta_i(M_{ik}) Z_i(M_{ik})\right)}{a_{ik}^{\text{in}} + a_{ik}^{\text{out}}}.\end{aligned} \tag{27}$$

Finally, we apply the divergence theorem to the first term on the RHS of (27) and arrive at the following quadrature for the cell average $\overline{S}_i^{(2)}$:

$$\begin{aligned}\overline{S}_i^{(2)} = \frac{g}{|T_i|} \sum_{k=1}^{3} \ell_{ik} \cos(\theta_{ik}) \Bigg[&\frac{a_{ik}^{\text{in}} \left(\frac{\eta_{ik}^2(M_{ik})}{2} - \eta_{ik}(M_{ik}) Z_{ik}(M_{ik})\right) + a_{ik}^{\text{out}} \left(\frac{\eta_i^2(M_{ik})}{2} - \eta_i(M_{ik}) Z_i(M_{ik})\right)}{a_{ik}^{\text{in}} + a_{ik}^{\text{out}}} \\ &- (\overline{\eta}_i - \overline{Z}_i) \frac{\eta_i(M_{ik}) + \eta_{ik}(M_{ik})}{2} \Bigg].\end{aligned} \tag{28}$$

Likewise, we obtain the quadrature for the cell average $\overline{S}_i^{(3)}$:

$$\begin{aligned}\overline{S}_i^{(3)} = \frac{g}{|T_i|} \sum_{k=1}^{3} \ell_{ik} \sin(\theta_{ik}) \Bigg[&\frac{a_{ik}^{\text{in}} \left(\frac{\eta_{ik}^2(M_{ik})}{2} - \eta_{ik}(M_{ik}) Z_{ik}(M_{ik})\right) + a_{ik}^{\text{out}} \left(\frac{\eta_i^2(M_{ik})}{2} - \eta_i(M_{ik}) Z_i(M_{ik})\right)}{a_{ik}^{\text{in}} + a_{ik}^{\text{out}}} \\ &- (\overline{\eta}_i - \overline{Z}_i) \frac{\eta_i(M_{ik}) + \eta_{ik}(M_{ik})}{2} \Bigg].\end{aligned} \tag{29}$$

Notice that since at "lake at rest" states $\eta_x \equiv \eta_y \equiv 0$, the quadratures (28), (29) satisfy (24), (25) as long as $\eta \equiv \eta_c$, $u \equiv v \equiv 0$.

Since the source term $\boldsymbol{K}$ in equation (8), does not affect the well-balanced property of the developed central-upwind scheme, we discretize its cell averages, $\{\overline{\boldsymbol{K}}_i\}$ in a straightforward manner by using the midpoint rule:

$$\overline{\boldsymbol{K}}_i = \boldsymbol{K}(x_i, y_i).$$

3.4. Time integration

The semi-discretization (14) is a system of time-dependent ODEs, which should be integrated using a stable and sufficiently accurate ODE solver. In our numerical experiments, we have used the third-order strong stability preserving (SSP) Runge–Kutta solver, see, e.g., [21,22].

The time step restriction is determined by the CFL condition (for details, see [30]) and can be expressed as

$$\Delta t = C_r \min_{i,k} \left[\frac{R_i}{\max(a_{ik}^{\text{in}}, a_{ik}^{\text{out}})} \right],$$

where C_r is the Courant number typically taken in the range $0 < C_r \le 1$ and R_i is the minimum distance from the centroid of the cell T_i to its edges.

4. Numerical experiments

In this section, we demonstrate the performance of the proposed central-upwind scheme on five test problems.

Example 1—small perturbation of a "lake at rest" state

This numerical example is a modification of the benchmark proposed in [35]. It is designed to test the ability of the designed scheme to accurately capture small perturbations of "lake at rest" states.

In this test, the computational domain is $[0, 2] \times [0, 1]$ and it is divided into 20 658 triangular cells. The initial conditions are

$$\eta(x,y,0)=\begin{cases}1.01, & \text{if } 0.05<x<0.15,\\ 1, & \text{otherwise,}\end{cases}\qquad u(x,y,0)\equiv v(x,y,0)\equiv 0,$$

$$c(x,y,0)\equiv 0.05,\qquad Z(x,y,0)=0.8\exp\Big[-5(x-0.9)^2-50(y-0.5)^2\Big].$$

We have used zero-order extrapolation at the right and left boundaries, while the solid wall boundary conditions have been implemented in the y-direction.

The gravity acceleration is set to $g=1$, the bed porosity is taken to be $p=0.3$, and the coefficient μ in equation (5) set to $\mu=0.001$. In this example, we do not use equation (7) to determine the settling velocity of particles, but instead we set it to $\omega_0=1$.

Fig. 3 (left) shows the contour lines of water surface for the right-going disturbance as it propagates past the hump at times $t=0.6, 0.9, 1.2, 1.5$ and 1.8, respectively. As one can see, complex small features of the flow are resolved in an oscillation-free manner and the results are in good agreement with the ones reported in [35]. To demonstrate the necessity and importance of the well-balanced property, we also apply a non-well-balanced central-upwind scheme to the same problem. The non-well-balanced scheme is obtained by replacing the bed-slope terms $\overline{S}_i^{(2)}$ and $\overline{S}_i^{(3)}$ in (28) and (29) by a straightforward midpoint rule discretization:

$$\overline{S}_i^{(2)}=-\eta(x_i,y_i)\frac{g}{|T_i|}\sum_{k=1}^{3}\ell_{ik}\cos(\theta_{ik})\frac{Z_i(M_{ik})+Z_{ik}(M_{ik})}{2},$$

$$\overline{S}_i^{(3)}=-\eta(x_i,y_i)\frac{g}{|T_i|}\sum_{k=1}^{3}\ell_{ik}\sin(\theta_{ik})\frac{Z_i(M_{ik})+Z_{ik}(M_{ik})}{2}.$$

The non-well-balanced solution computed on the same grid is presented in Fig. 3 (right). It can be clearly observed that spurious waves are generated by the non-well-balanced scheme at the plateau of the hump. Moreover, the spurious waves are of approximately the same magnitude as the physical waves, which suggests that the non-well-balanced scheme should be used on much finer grid only, which would make it impractical.

Fig. 4 shows the 1-D slice along the line $y=0.5$ of both the water surface and bed evolutions (the latter occurs due to the sediment deposition) at the same times $t=0.6, 0.9, 1.2, 1.5$ and 1.8. It should be observed that even in the presence of sediment concentration, the well-balanced property of the proposed scheme has prevented numerical oscillations that are typically observed when the computation is conducted using a non-well-balanced scheme.

Example 2—sand deposition in quiescent water

This test is designed to verify that the added source terms will not affect the well-balanced property in quiescent water with uniform sediment deposition.

We take the computational domain $[0,2]\times[0,1]$, which is divided into 3628 triangular cells, set the following initial conditions:

$$\eta(x,y,0)\equiv 1,\quad u(x,y,0)\equiv v(x,y,0)\equiv Z(x,y,0)\equiv 0,$$

$$c(x,y,0)=0.7\exp\Big[-5(x-0.9)^2-50(y-0.5)^2\Big],$$

and use zero-order extrapolation at all of the boundaries.

We also use the following values of the parameters: the gravity acceleration is $g=9.8$, the bed porosity is $p=0.28$, the sediment diameter is $d=0.01$, the density of sediment particles is $\rho_s=2400$, the density of water is $\rho_f=1000$, and the coefficient μ in equation (5) is $\mu=0$.

In Fig. 5, we show the quiescent water surface and bed profile at a large time $t=100$. As one can see, no oscillations are developed at the quiescent water surface, so that the sediment deposition does not affect the numerical "lake at rest" steady state. The 1-D slice along the line $y=0.5$ of the obtained results is shown in Fig. 6.

Example 3—dam-break flow in a long channel over erodible bed

This test is performed to investigate the advantage of the proposed central-upwind scheme applied to the fully coupled system (1)–(5) over a simpler partially coupled approach, in which the central-upwind scheme is applied to the first four equations (1)–(4) only, while the equation for the bed evolution (5) is solved using an upwind method as it is described below.

For simplicity, the sediment entrainment effects are deactivated so that we take $E\equiv D\equiv 0$.

In the partially coupled method, the first four conservative quantities, η, hu, hv and hc, are evolved in time by solving the same ODE system (14), but with different one-sided speeds of propagation, which are now obtained using the largest and smallest eigenvalues of the matrix

$$\widetilde{V}_{ik}:=\cos(\theta_{ik})\widetilde{A}(\boldsymbol{U}(M_{ik}))+\sin(\theta_{ik})\widetilde{B}(\boldsymbol{U}(M_{ik})),$$

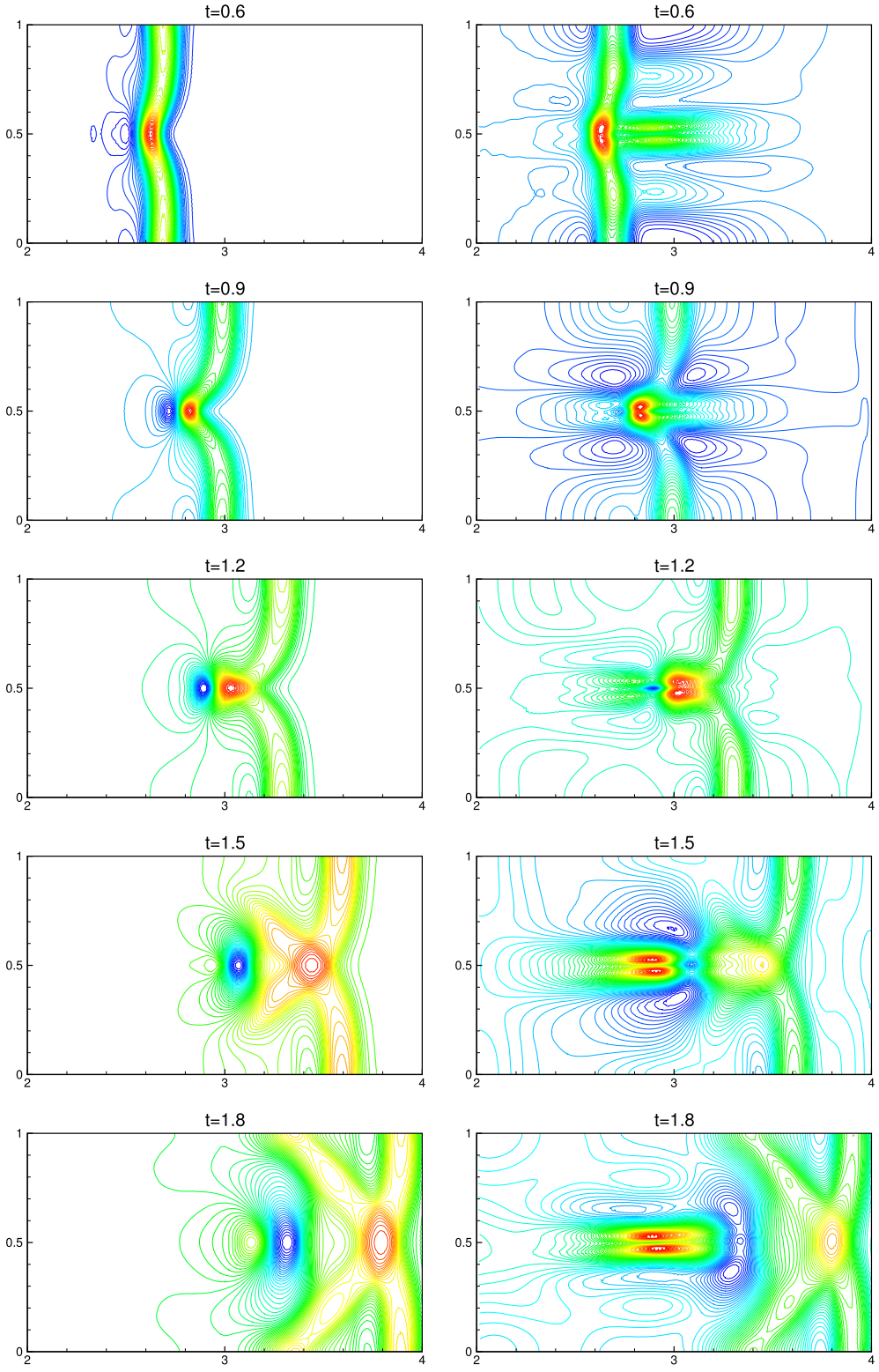

Fig. 3. Example 1: water surface η computed by well-balanced (left) and non-well-balanced (right) schemes.

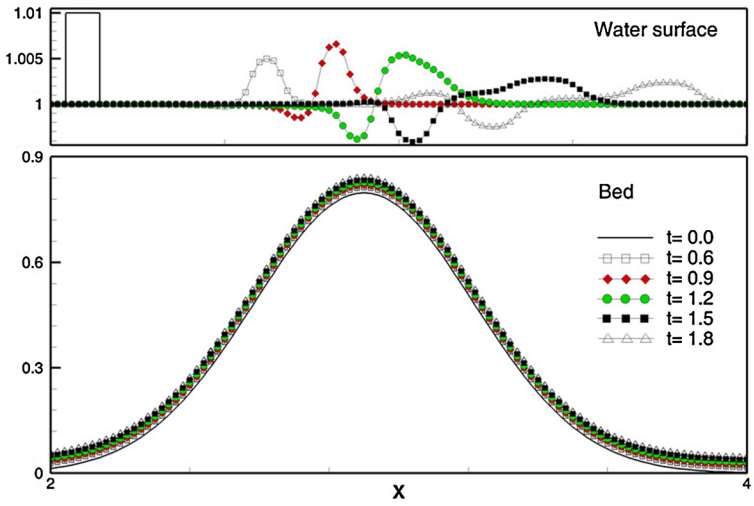

Fig. 4. Example 1: 1-D slices of the water surface η and bed Z along the line $y = 0.5$.

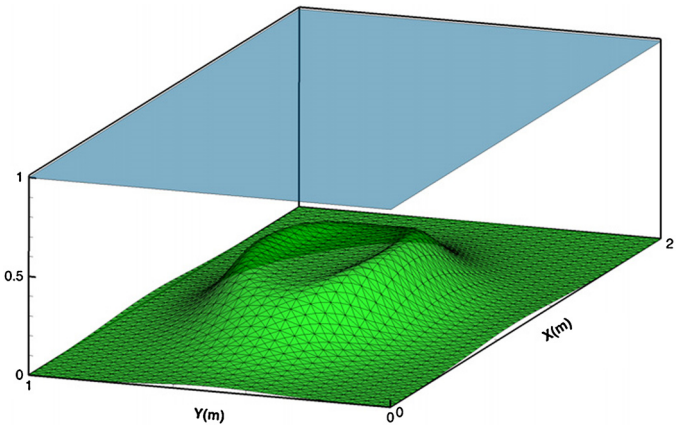

Fig. 5. Example 2: bed Z and quiescent water surface η at $t = 100$.

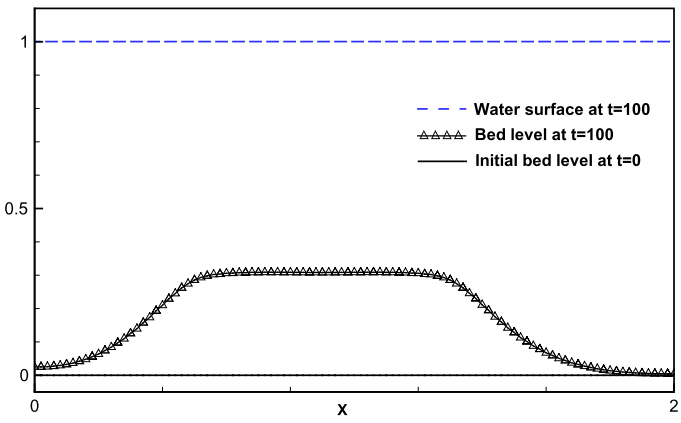

Fig. 6. Example 2: 1-D slice along the line $y = 0.5$ of the results reported in Fig. 5.

where

$$\widetilde{A}(\boldsymbol{U})=\begin{pmatrix} 0 & 1 & 0 & 0\\ -\dfrac{(hu)^2}{(\eta-Z)^2}+g(\eta-Z) & \dfrac{2hu}{\eta-Z} & 0 & 0\\ -\dfrac{(hu)(hv)}{(\eta-Z)^2} & \dfrac{hv}{\eta-Z} & \dfrac{hu}{\eta-Z} & 0\\ -\dfrac{(hu)(hc)}{(\eta-Z)^2} & \dfrac{hc}{\eta-Z} & 0 & \dfrac{hu}{\eta-Z} \end{pmatrix},$$

and

$$\widetilde{B}(\boldsymbol{U})=\begin{pmatrix} 0 & 0 & 1 & 0\\ -\dfrac{(hu)(hv)}{(\eta-Z)^2} & \dfrac{hv}{\eta-Z} & \dfrac{hu}{\eta-Z} & 0\\ -\dfrac{(hv)^2}{(\eta-Z)^2}+g(\eta-Z) & 0 & \dfrac{2hv}{\eta-Z} & 0\\ -\dfrac{(hv)(hc)}{(\eta-Z)^2} & 0 & \dfrac{hc}{\eta-Z} & \dfrac{hv}{\eta-Z} \end{pmatrix}.$$

Unlike the case of a fully coupled model, the eigenvalues of $\widetilde{V}_{ik}(\boldsymbol{U}_i(M_{ik}))$ can be computed analytically and they are

$$\lambda_{1,4}=\frac{hu}{\eta-Z}\cos(\theta_{ik})+\frac{hv}{\eta-Z}\sin(\theta_{ik})\pm\sqrt{g(\eta-Z)},$$
$$\lambda_2=\lambda_3=\frac{hu}{\eta-Z}\cos(\theta_{ik})+\frac{hv}{\eta-Z}\sin(\theta_{ik}).$$

The bottom topography function is evolved in time by applying the semi-discrete upwind discretization to equation (5):

$$\begin{aligned}\frac{d\overline{Z}_i}{dt}=&-\frac{\mu}{|T_i|(1-p)}\sum_{k=1}^{3}\ell_{ik}\cos(\theta_{ik})\Big[\beta_{ik}\,u_{ik}(M_{ik})\big(u_{ik}^2(M_{ik})+v_{ik}^2(M_{ik})\big)\\ &\qquad(1-\beta_{ik})u_i(M_{ik})\big(u_i^2(M_{ik})+v_i^2(M_{ik})\big)\Big]\\ &-\frac{\mu}{|T_i|(1-p)}\sum_{k=1}^{3}\ell_{ik}\cos(\theta_{ik})\Big[\beta_{ik}\,v_{ik}(M_{ik})\big(u_{ik}^2(M_{ik})+v_{ik}^2(M_{ik})\big)\\ &\qquad(1-\beta_{ik})v_i(M_{ik})\big(u_i^2(M_{ik})+v_i^2(M_{ik})\big)\Big],\end{aligned}$$

where

$$\beta_{ik}=\begin{cases}0, & \dfrac{u_{ik}(M_{ik})+u_i(M_{ik})}{2}\cos(\theta_{ik})+\dfrac{v_{ik}(M_{ik})+v_i(M_{ik})}{2}\sin(\theta_{ik})\ge 0,\\ 1, & \text{otherwise.}\end{cases}$$

In this numerical test, we simulate a dam-break flow over erodible bed. The computational domain $[0,40]\times[0,0.5]$ is divided into 2560 triangular cells. The initial conditions are

$$\eta(x,y,0)=\begin{cases}3.1, & x\le 20,\\ 0.2, & x>20,\end{cases}\qquad u(x,y,0)\equiv v(x,y,0)\equiv c(x,y,0)\equiv Z(x,y,0)\equiv 0,$$

and zero-order extrapolation is used at all of the boundaries. The parameter values are $g=9.8$, $p=0.28$ and $\mu=0.001$.

In Fig. 7, we show the bed profile computed at $t=1$ using the central-upwind scheme applied to both fully coupled and partially coupled models. As one can clearly see, even under a high-energetic flow considered in this example, the fully coupled model can predict a stable bed erosion process and leads to a smooth and physically expectable bed profile. On the contrary, the use of the partially coupled model results in an unphysical and oscillatory bed profile.

Example 4—1-D anti-dune evolution

In this numerical test, we simulate a case with a configuration which allows the occurrence of the anti-dune phenomenon, see [4]. The computational domain in $[0,24]$ and it is discretized on the mesh with an average size $\Delta x=0.1$. The initial topography contains a bump and is given by

$$Z(x,0)=\begin{cases}0.2-0.05(x-10)^2, & \text{if } 8\le x\le 12,\\ 0, & \text{otherwise.}\end{cases}$$

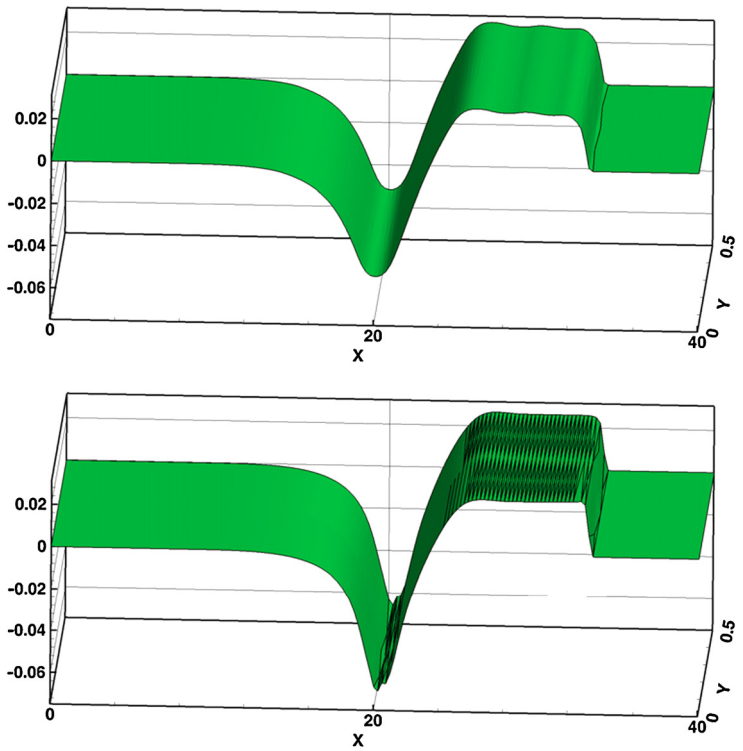

Fig. 7. Example 3: bed profile $Z(x, y, 1)$ computed using the central-upwind scheme applied to the fully coupled (top) and partially coupled (bottom) models.

The inflow discharge is uniform and set to be $q_0 = 1.7$. The water height of the inflow is the stationary supercritical profile determined by Bernoulli's law

$$\begin{cases} \dfrac{q_0^2}{2gh^2} + h + Z = H_0, \\ q(x,t) = q_0, \end{cases}$$

where $H_0 = q_0^2/(2gh_0^2) + h_0 + Z(0,0)$ is the total hydraulic head at inflow, and the water height at inflow is $h_0 = 0.5$. In this test, we set $A_g = \mu/(1-p) = 0.001$, $g = 9.8$ and $E \equiv D \equiv 0$.

In Fig. 8, we show the computed bed evolution and water level at times $t = 0$, 15 and 30. As one can observe, the dune migrates counter to the flow direction because the sediment is deposited on the upstream side and eroded from the downstream side. It shows that the proposed model has the ability to accurately simulate the anti-dune phenomenon which occurs in supercritical regimes.

Example 5—partial dam-break flow over mobile bed

In the last numerical example, we demonstrate the performance of the proposed central-upwind scheme on a 2-D dam break problem with rapidly varying unsteady flow and rapid bed evolution. This test problem is based on the numerical test that was first introduced in [18] and then widely used as a benchmark, see, e.g., [2,3,49,53,58]. The original case is mostly applied on an initially wet and fixed bed, which has been modified in the current study by adding bed evolution.

We consider the domain $[0, 200] \times [0, 200]$ with the rectangular dam located in $[95, 105] \times [0, 200]$. The initial conditions are

$$\eta(x,y,0) = \begin{cases} 6.8, & x \le 95, \\ 1, & x \ge 105, \end{cases} \qquad u(x,y,0) \equiv v(x,y,0) \equiv c(x,y,0) \equiv Z(x,y,0) \equiv 0.$$

At time $t = 0$, a breach in the dam at $[95, 105] \times [85, 160]$ is assumed to form instantaneously and the water starts flowing through the breach. The computational domain covered with 10 508 triangular cells is outlined in Fig. 9. Notice that at the breach region where the gradients of the water depth are large and intense sediment transport occurs, the mesh is refined to obtain high resolution. The outlet boundary condition is set at $x = 200$, while the solid wall boundary conditions are used at all other boundaries. In this example, we use the following parameter values: $g = 9.8$, $p = 0.28$, $d = 0.01$, $\rho_s = 2400$, $\rho_f = 1000$, $\mu = 0.001$, and compute the solution up to time $t = 8$. During the modeling process, a shock wave forms and propagates downstream and a depression wave spreads upstream.

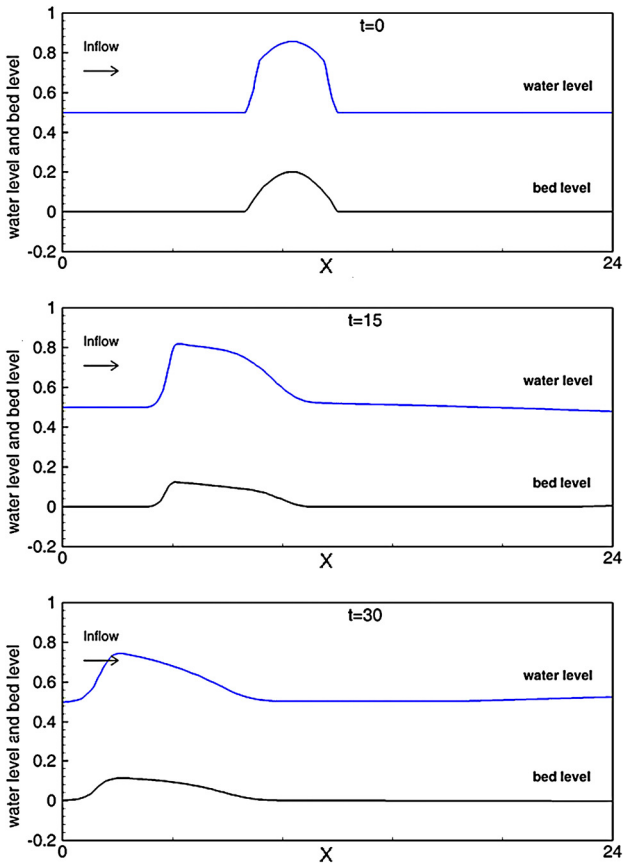

Fig. 8. Example 4: water level (η) and bed profile (Z) computed by the proposed central-upwind scheme at times $t = 0$, 15 and 30.

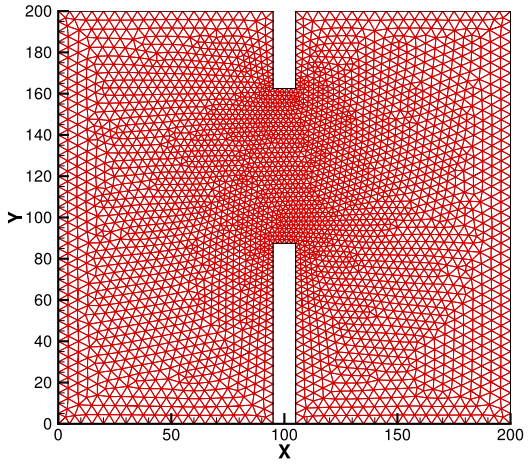

Fig. 9. Example 5: computational domain and its unstructured triangulation.

We first solve the shallow water system (1)–(3) assuming that the bed is fixed, that is, $Z_t \equiv Z_x \equiv Z_y \equiv 0$. The predicted water level and velocity distribution are shown in Fig. 10: The obtained results are in good agreement with those reported in [9,48,53,57].

We then consider a general case of an erodible bed and solve the system (1)–(5) using both the fully and partially coupled models. For both models the computed water surfaces (not shown here for the sake of brevity) contain no spurious oscillations and the obtained flow patterns are quite similar.

However, the bed elevations predicted by the fully and partially coupled models are very different, as one can see in Fig. 11, where we show the bottom topography snapshots at times $t = 4$, 6 and 8. It can be clearly observed that at the

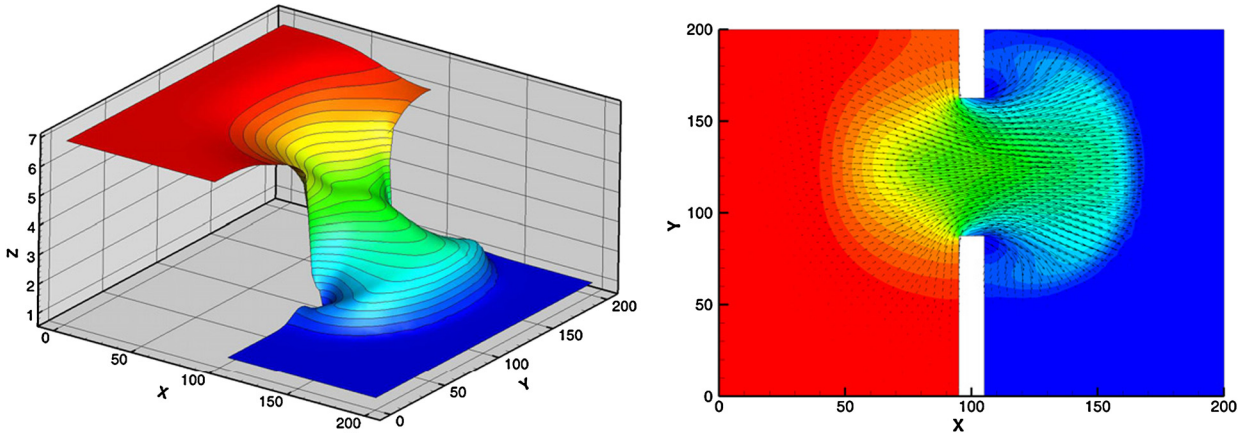

Fig. 10. Example 5 with fixed bed: water level $\eta(x, y, 8)$; surface plot (left) and contour plot with the velocity field (right).

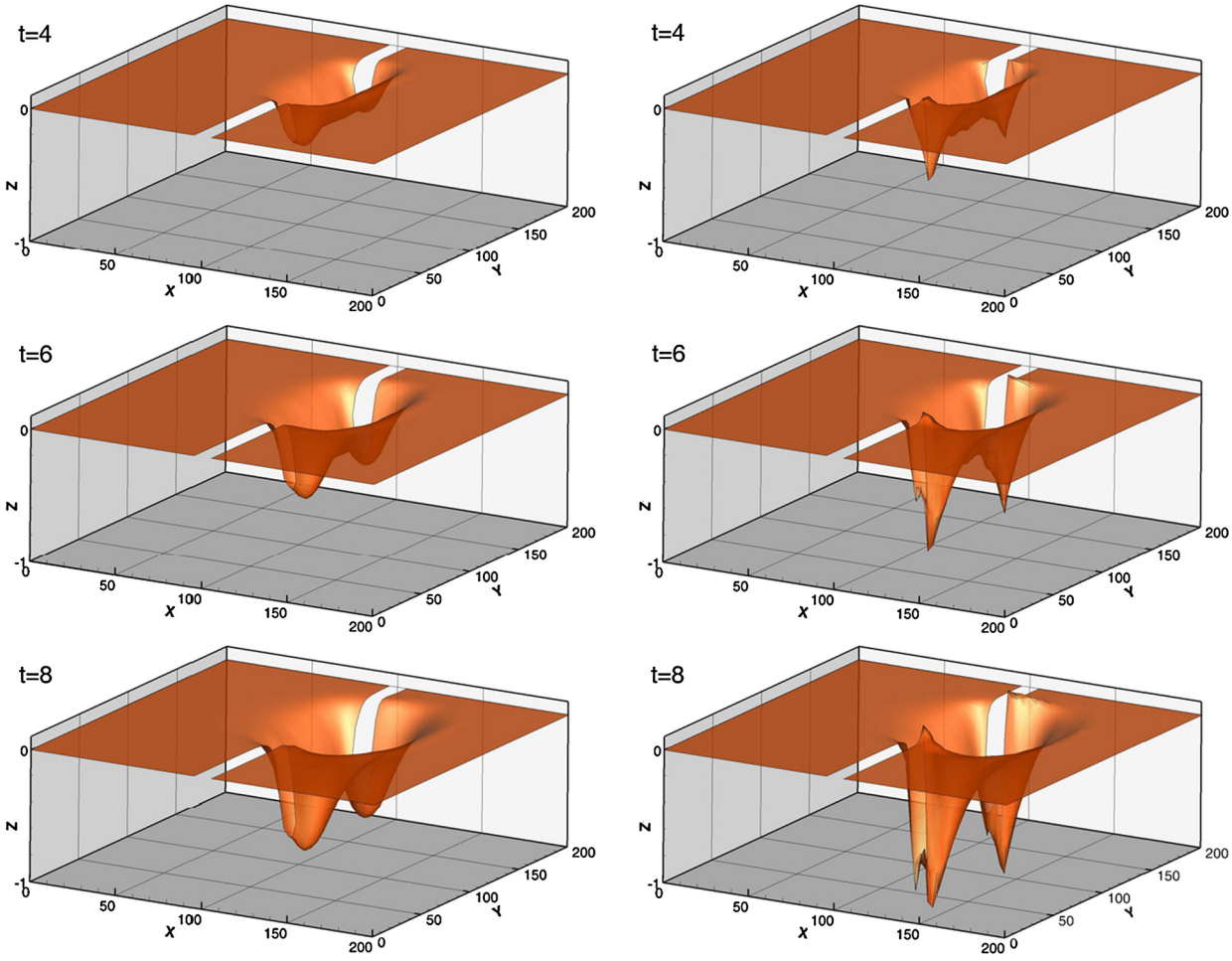

Fig. 11. Example 5: bed evolution computed using the proposed fully coupled model (left) and partially coupled model (right).

corners of both sides of the breach where intense scouring and sediment entrainment are induced by strong vortices, the partially coupled model produces very sharp unphysical scouring holes and slight oscillations (see Fig. 11 (right)), which may develop spurious oscillations when a flow with higher energy is applied. In contrast with the results obtained using the partially coupled model, the bed elevations predicted using the fully coupled model are more accurate and smoother at the corners of the breach and no unphysical scouring and oscillations can be observed in Fig. 11 (left).

5. Conclusion

In this paper, we have proposed and studied a fully coupled model that contains the shallow water system, sediment transport equation and bed evolution equation. We have developed a well-balanced, second-order, semi-discrete central-upwind scheme on unstructured triangular grids. The scheme has been tested on a number of numerical examples, which have demonstrated that the developed central-upwind scheme is an efficient and stable tool for solving the proposed fully coupled hyperbolic system that models shallow water flows with intense sediment exchange and bed erosion process.

Some of the major conclusions have been drawn:

1. Applying the Lagrange theorem efficiently reduces the cost of finding the smallest and largest eigenvalues of the complicated 5×5 Jacobian. By comparing the results of the fully and partially coupled models, one may claim that the upper/lower bounds on the largest/smallest eigenvalues obtained using the Lagrange theorem are quite sharp;
2. The model proposed in this paper couples the bed evolution equation into the hyperbolic system, which leads to more stable and accurate results. The bed evolution process is less oscillatory compared with a partially coupled model, especially when intense scouring and sediment exchange occur. This implies that the proposed fully coupled model is advantageous for highly energetic flows like the dam-break one and fluvial flood;
3. The well-balanced discretization proposed in the current paper is designed for discontinuous Z, approximated using a (generically discontinuous) piecewise polynomial, which is evolved in the framework of a finite-volume methods. This approach proves to be very robust and accurate.

Acknowledgements

Xin Liu, Abdolmajid Mohammadian and Julio Angel Infante Sedano were supported by the Natural Science and Engineering Council of Canada (NSERC) and NPRP grant 4-935-2-354 from the Qatar National Research Fund (a member of Qatar Foundation). The work of Alexander Kurganov was supported in part by NSF grant DMS-1216957 and ONR grant N00014-12-1-0833.

References

[1] R. Abgrall, On essentially non-oscillatory schemes on unstructured meshes: analysis and implementation, J. Comput. Phys. 114 (1994) 45–58.
[2] F. Alcrudo, P. Garcia-Navarro, A high-resolution Godunov-type scheme in finite volumes for the 2D shallow-water equations, Int. J. Numer. Methods Fluids 16 (6) (1993) 489–505.
[3] K. Anastasiou, C.T. Chan, Solution of the 2D shallow water equations using the finite volume method on unstructured triangular meshes, Int. J. Numer. Methods Fluids 24 (11) (1997) 1225–1245.
[4] E. Audusse, O. Delestre, M.H. Le, M. Masson-Fauchier, P. Navaro, R. Serra, Parallelization of a relaxation scheme modelling the bedload transport of sediments in shallow water flow, in: ESAIM: Proceedings, vol. 43, EDP Sciences, 2013, pp. 80–94.
[5] F. Benkhaldoun, I. Elmahi, S. Sari, M. Seaïd, A two-dimensional finite volume solution of dam-break hydraulics over erodible sediment beds, in: Finite Volumes for Complex Applications. VI. Problems & Perspectives. Vols. 1, 2, in: Springer Proc. Math., vol. 4, Springer, Heidelberg, 2011, pp. 875–891.
[6] C. Biscarini, S. Di Francesco, P. Manciola, CFD modelling approach for dam break flow studies, Hydrol. Earth Syst. Sci. 14 (4) (2010) 705–718.
[7] P. Brufau, P. Garcia-Navarro, Two-dimensional dam break flow simulation, Int. J. Numer. Methods Fluids 33 (1) (2000) 35–57.
[8] S. Bryson, Y. Epshteyn, A. Kurganov, G. Petrova, Well-balanced positivity preserving central-upwind scheme on triangular grids for the Saint-Venant system, Modél. Math. Anal. Numér. 45 (3) (2011) 423–446.
[9] V. Caleffi, A. Valiani, A. Zanni, Finite volume method for simulating extreme flood events in natural channels, J. Hydraul. Res. 41 (2) (2003) 167–177.
[10] Z. Cao, P.A. Carling, Mathematical modelling of alluvial rivers: reality and myth. Part 2: Special issues, in: Proceedings of the Institution of Civil Engineers–Water Maritime and Engineering, vol. 154, 2002, pp. 297–308.
[11] Z. Cao, G. Pender, S. Wallis, P. Carling, Computational dam-break hydraulics over erodible sediment bed, J. Hydraul. Eng. 128 (5) (2002) 460–472.
[12] H. Capart, D.L. Young, Formation of jump by the dam-break wave over a granular bed, J. Fluid Mech. 372 (1998) 165–187.
[13] M.J. Castro Díaz, E.D. Fernández-Nieto, A.M. Ferreiro, Sediment transport models in shallow water equations and numerical approach by high order finite volume methods, Comput. Fluids 37 (3) (2008) 299–316.
[14] A. Chertock, A. Kurganov, Z. Qu, T. Wu, Three-layer approximation of two-layer shallow water equations, Math. Model. Anal. 18 (5) (2013) 675–693.
[15] I. Christov, B. Popov, New nonoscillatory central schemes on unstructured triangulations for hyperbolic systems of conservation laws, J. Comput. Phys. 227 (2008) 5736–5757.
[16] L.J. Durlofsky, B. Engquist, S. Osher, Triangle based adaptive stencils for the solution of hyperbolic conservation laws, J. Comput. Phys. 98 (1992) 64–73.
[17] S. Fagherazzi, T. Sun, Numerical simulations of transportational cyclic steps, Comput. Geosci. 29 (9) (2003) 1143–1154.
[18] R.J. Fennema, M.H. Chaudhry, Explicit methods for 2-D transient free surface flows, J. Hydraul. Eng. 116 (8) (1990) 1013–1034.
[19] R.M.L. Ferreira, J.G.A.B. Leal, 1D mathematical modelling of the instantaneous dam-break flood wave over mobile bed: application of TVD and flux-splitting schemes, in: Proc., European Concerted Action on Dam-Break Modeling, 1998, pp. 175–222.
[20] L. Fraccarollo, A. Armanini, A semi-analytical solution for the dam-break problem over a movable bed, in: Proc., European Concerted Action on Dam-Break Modeling, 1998, pp. 145–152.
[21] S. Gottlieb, D. Ketcheson, C.-W. Shu, Strong Stability Preserving Runge–Kutta and Multistep Time Discretizations, World Scientific Publishing Co. Pte. Ltd., Hackensack, NJ, 2011.
[22] S. Gottlieb, C.-W. Shu, E. Tadmor, Strong stability-preserving high-order time discretization methods, SIAM Rev. 43 (2001) 89–112.
[23] A.J. Grass, Sediment transport by waves and currents, Report No. FL29, SERC London Cent. Mar. Technol., 1981.
[24] P. Hu, Z. Cao, G. Pender, G. Tan, Numerical modelling of turbidity currents in the Xiaolangdi reservoir, Yellow River, China, J. Hydrol. 464 (2012) 41–53.
[25] J. Hudson, P.K. Sweby, Formulations for numerically approximating hyperbolic systems governing sediment transport, J. Sci. Comput. 19 (1) (2003) 225–252.
[26] P. Jawahar, H. Kamath, A high-resolution procedure for Euler and Navier–Stokes computations on unstructured grids, J. Comput. Phys. 164 (1) (2000) 165–203.

[27] A. Kurganov, D. Levy, Central-upwind schemes for the Saint-Venant system, Modél. Math. Anal. Numér. 36 (2002) 397–425.
[28] A. Kurganov, C.-T. Lin, On the reduction of numerical dissipation in central-upwind schemes, Commun. Comput. Phys. 2 (2007) 141–163.
[29] A. Kurganov, S. Noelle, G. Petrova, Semi-discrete central-upwind scheme for hyperbolic conservation laws and Hamilton–Jacobi equations, SIAM J. Sci. Comput. 23 (2001) 707–740.
[30] A. Kurganov, G. Petrova, Central-upwind schemes on triangular grids for hyperbolic systems of conservation laws, Numer. Methods Partial Differ. Equ. 21 (2005) 536–552.
[31] A. Kurganov, G. Petrova, A second-order well-balanced positivity preserving central-upwind scheme for the Saint-Venant system, Commun. Math. Sci. 5 (2007) 133–160.
[32] A. Kurganov, G. Petrova, Central-upwind schemes for two-layer shallow equations, SIAM J. Sci. Comput. 31 (2009) 1742–1773.
[33] A. Kurganov, E. Tadmor, New high resolution central schemes for nonlinear conservation laws and convection–diffusion equations, J. Comput. Phys. 160 (2000) 241–282.
[34] J.L. Lagrange, Traité de la résolution des équations numériques, Paris, 1798. Reprinted in Œuvres, 8, 1879.
[35] R.J. LeVeque, Balancing source terms and flux gradients in high-resolution Godunov methods: the quasi-steady wave-propagation algorithm, J. Comput. Phys. 146 (1) (1998) 346–365.
[36] S. Li, C.J. Duffy, Fully coupled approach to modeling shallow water flow, sediment transport, and bed evolution in rivers, Water Resour. Res. 47 (3) (2011).
[37] L. Liang, J. Ni, A.G.L. Borthwick, B.D. Rogers, Simulation of dike-break processes in the Yellow River, Sci. China, Ser. E, Tech. Sci. 45 (6) (2002) 606–619.
[38] M. Mignotte, D. Stefanescu, On an estimation of polynomial roots by Lagrange, Technical Report 025/2002, IRMA Strasbourg, 2002, pp. 1–17, http://hal.archives-ouvertes.fr/hal-00129675/en/.
[39] J. Murillo, P. García-Navarro, An Exner-based coupled model for two-dimensional transient flow over erodible bed, J. Comput. Phys. 229 (23) (2010) 8704–8732.
[40] D. Pan, J.-C. Cheng, Upwind finite-volume Navier–Stokes computations on unstructured triangular meshes, AIAA J. 31 (9) (1993) 1618–1625.
[41] D. Pritchard, A.J. Hogg, On sediment transport under dam-break flow, J. Fluid Mech. 473 (2002) 265–274.
[42] A. Serrano-Pacheco, J. Murillo, P. Garcia-Navarro, An Exner-based coupled model for two-dimensional transient flow over erodible bed, J. Hydraul. Res. 50 (2) (2012) 154–163.
[43] G. Simpson, S. Castelltort, Coupled model of surface water flow, sediment transport and morphological evolution, Comput. Geosci. 32 (10) (2006) 1600–1614.
[44] S. Soares Frazão, D. Lories, S. Taminiau, Y. Zech, Dam-break flow in a channel with a sudden enlargement, in: XXX IAHR Congress, Thessaloniki, Greece, 2003, pp. 25–31.
[45] S. Soares Frazão, Y. Zech, HLLC scheme with novel wave-speed estimators appropriate for two-dimensional shallow-water flow on erodible bed, Int. J. Numer. Methods Fluids 66 (8) (2011) 1019–1036.
[46] T. Tingsanchali, C. Chinnarasri, Numerical modelling of dam failure due to flow overtopping, Hydrol. Sci. J. 46 (1) (2001) 113–130.
[47] A. Valiani, V. Caleffi, A. Zanni, Case study: Malpasset dam-break simulation using a two-dimensional finite volume method, J. Hydraul. Eng. 128 (5) (2002) 460–472.
[48] J.-W. Wang, R.-X. Liu, A comparative study of finite volume methods on unstructured meshes for simulation of 2D shallow water wave problems, Math. Comput. Simul. 53 (3) (2000) 171–184.
[49] J.-W. Wang, R.-X. Liu, The composite finite volume method on unstructured triangular meshes for 2D shallow water equations, Int. J. Numer. Methods Fluids 37 (2001) 933–949.
[50] M. Wierse, A new theoretically motivated higher order upwind scheme on unstructured grids of simplices, Adv. Comput. Math. 7 (3) (1997) 303–335.
[51] W. Wu, S.S. Wang, One-dimensional modeling of dam-break flow over movable beds, J. Hydraul. Eng. 133 (1) (2007) 48–58.
[52] J. Xia, B. Lin, R.A. Falconer, G. Wang, Modelling dam-break flows over mobile beds using a 2D coupled approach, Adv. Water Resour. 33 (2) (2010) 171–183.
[53] J. Xia, B. Lin, R.A. Falconer, G. Wang, Modelling dam-break flows over mobile beds using a 2D coupled approach, Adv. Water Resour. 33 (2) (2010) 171–183.
[54] Z.Y. Yue, Z.X. Cao, X. Li, T. Che, Two-dimensional coupled mathematical modeling of fluvial processes with intense sediment transport and rapid bed evolution, Sci. China, Ser. G, Phys. Mech. Astron. 51 (9) (2008) 1427–1438.
[55] R. Zhang, J. Xie, Sedimentation Research in China: Systematic Selections, China Water and Power Press, 1993.
[56] X.Z. Zhang, G.Q. Wang, Flow analysis and scour computation of the dike-break, J. Sediment. Res. 1 (2002) 18–24.
[57] D.H. Zhao, H.W. Shen, J.S. Lai, G.Q. Tabios III, Approximate Riemann solvers in FVM for 2D hydraulic shock wave modeling, J. Hydraul. Eng. 122 (12) (1996) 692–702.
[58] D.H. Zhao, H.W. Shen, G.Q. Tabios III, J.S. Lai, W.Y. Tan, Finite-volume two-dimensional unsteady-flow model for river basins, J. Hydraul. Eng. 120 (7) (1994) 863–883.
[59] J.G. Zhou, D.M. Causon, C.G. Mingham, D.M. Ingram, Numerical prediction of dam-break flows in general geometries with complex bed topography, J. Hydraul. Eng. 130 (4) (2004) 332–340.
[60] C. Zoppou, S. Roberts, Numerical solution of the two-dimensional unsteady dam break, Appl. Math. Model. 24 (7) (2000) 457–475.